

## Chapter 3

THE  $[B_{12}(OR)_{12}]^{1+}$  CATION

A manuscript based on the work presented in this chapter is being prepared by Stauber, J. M.; Schwan, L. J.; Xhang, X.; Axtell, J. C.; Jung, D.; McNicholas, B. J.; Oyala, P. H.; Winkler, J. R.; Miller, T. F.; Gray H. B.; Spokoyny, A.M. Evidence for the Existence of Cationic Dodecaborate-based Clusters.

*Chapter 3 discusses our discovery of a  $[B_{12}(OR)_{12}]^{1+}$  species and initial attempts at isolating and characterizing this cationic cluster. Our investigations started with the observation of a third oxidation wave in the cyclic voltammogram of  $B_{12}(OEt)_{12}$  (**4**,  $Et = C_2H_5$ ), which we assigned to a super-oxidized  $[4]^{1+}$  species. Further electrochemical investigation of **4** in 0.2 M TBAPF<sub>6</sub> dichloromethane electrolyte showed three reversible waves at  $E_{1/2}(2-/1-) = -1.08$  V,  $E_{1/2}(0/1-) = -0.454$  V and  $E_{1/2}(1+/0) = +0.747$  V. Additionally, a strong irreversible wave is observed at  $> +1.2$  V, which could indicate further oxidation to  $[4]^{2+}$ . Electrochemically derived visible spectra of  $[4]^{1+}$  show a new broad absorption band at 707 nm and a strong 455 nm band (slightly blue-shifted from the 460 nm band of the neutral species). Preliminary attempts to chemically isolate  $[4]^{1+}$  indicated that tris(4-bromophenyl)ammoniumyl hexachloroantimonate was able to oxidize **4**, but not sufficiently strong for isolation of the cation. Using the more powerful oxidant tris(2,4-dibromophenyl)ammoniumyl hexachloroantimonate, we were able to isolate  $[B_{12}(OC_2H_2^iPr)_{12}][SbCl_6]$  (**5**)[ $SbCl_6$ ]. The isolated salts are not of sufficient purity for spectroscopic characterization; however, we were able to collect EPR spectra of  $[4]^{1+}$  and  $[4]^{1+}$  in-situ generated by addition of a substoichiometric amount of tris(2,4-dibromophenyl)ammoniumyl hexachloroantimonate. The EPR spectrum indicates a delocalized SOMO, similar to what has been reported for the anionic hypocloso- $[B_{12}]$  clusters.*

### 3.1 Introduction

Early theoretical predictions by Longuet-Higgins and Lipscomb suggested that dodecaborate ( $[B_{12}H_{12}]$ ) would not be stable as a neutral  $B_{12}H_{12}$  species but might be stable in its dianionic  $[B_{12}H_{12}]^{2-}$  state. These predictions considered a cluster in icosahedral ( $I_h$ ) symmetry, where the highest occupied molecular orbital (HOMO) is a four-fold degenerate  $g_u$  set. Neutral or monoanionic dodecaborates do not have enough electrons to fill the HOMO( $g_u$ ), suggesting that these species would be unstable due to an energetically unfavorable open-shell configuration.<sup>1-7</sup> Lipscomb and co-workers were the first to confirm the existence of a stable dodecaborate through their isolation and structural characterization of *closo*- $[B_{12}H_{12}]^{2-}$ . Later work has confirmed that oxidation of *closo*- $[B_{12}H_{12}]^{2-}$  leads to cluster decomposition or dimerization.<sup>8</sup> Wade generalized these results through the so-called ‘Wade’s rules’, which predict the structure of polyhedral molecules based on the number of skeletal bonding electron pairs.<sup>9,10</sup>

Over the past two decades, a range of dodecaborate derivatives have been isolated as hypoelectronic *hypocloso*- $[B_{12}]^{1-}$  and *hypercloso*- $B_{12}^0$  species ( $B_{12}$  denotes a generic dodecaborate cluster). Hawthorne first reported the isolation of *hypocloso*- $[B_{12}Me_{12}]^{1-}$  ( $Me = CH_3$ ), followed by *hypocloso*- $[B_{12}(OBz)_{12}]^{1-}$  and *hypercloso*- $B_{12}(OBz)_{12}$  ( $Bz = CH_2C_6H_5$ ).<sup>11,12</sup> Later work showed that perhydroxylated and perhalogenated dodecaborates could also be isolated as salts of *hypocloso*- $[B_{12}(OH)_{12}]^{1-}$  and *hypocloso*- $[B_{12}X_{12}]^{1-}$  ( $X = F, Cl, Br$ ).<sup>13,14</sup> A key breakthrough came when Spokoyny and co-workers discovered a more convenient method for rapid synthesis of *hypercloso*- $B_{12}(OR)_{12}$ .<sup>15</sup> The ability to readily produce large quantities of these compounds enabled in-depth exploration of their potential applications, most importantly the photopolymerization studies

discussed in Appendix A, as well as recent reports on their use in charge-storage devices and as dopants in conducting polymers.<sup>16-19</sup>

The stability of hypoelectronic *hypocloso*-[B<sub>12</sub>]<sup>1-</sup> and *hypercloso*-B<sub>12</sub><sup>0</sup> species have been attributed to three factors: (1) a structural distortion lowering the symmetry from I<sub>h</sub> to D<sub>3d</sub> or T<sub>d</sub>, which breaks the degeneracy of the HOMO(g<sub>u</sub>) to lower the overall cluster energy, (2) steric protection of the cluster-confined frontier orbitals by bulky substituents and (3) electron donation from the substituents into the B-B bonding frontier orbitals. The effect of the structural distortion is shown in Figure 3.1 (assuming D<sub>3d</sub> symmetry). Breaking of the g<sub>u</sub> degeneracy yields a non-degenerate a<sub>1u</sub> singly occupied molecular orbital (SOMO) in the case of *hypocloso*-[B<sub>12</sub>]<sup>1-</sup> or lowest unoccupied molecular orbital (LUMO) in the case of *hypercloso*-B<sub>12</sub><sup>0</sup>. Raising the energy of the a<sub>1u</sub> and lowering the energy of the fully occupied e<sub>g</sub> set leads to an energetically favorable state, stabilizing the cluster.<sup>15-17,20</sup> The role of electron donation is likely a major contributor, which will be discussed in more detail in Chapter 4.

Dodecaborate clusters oxidized beyond the *hypercloso*-B<sub>12</sub><sup>0</sup> state have so far not been reported. The current paradigm states that that removal of an electron from the HOMO(a<sub>2u</sub>) of *hypercloso*-B<sub>12</sub><sup>0</sup> would undoubtedly lead to cluster decomposition. Here, we show that a super-oxidized cationic [B<sub>12</sub>]<sup>1+</sup> state can be generated from B<sub>12</sub>(OR)<sub>12</sub> when R = alkyl. Both electrochemical and chemical means have been used to generate [B<sub>12</sub>(OEt)<sub>12</sub>]<sup>1+</sup> and [B<sub>12</sub>(OC<sub>2</sub>H<sub>4</sub><sup>i</sup>Pr)<sub>12</sub>]<sup>1+</sup> (Et = CH<sub>2</sub>CH<sub>3</sub>, <sup>i</sup>Pr = isopropyl). These observations open up for interesting discussions on what the oxidation limit of dodecaborates is and what types of reactivities these super-oxidized states can access.

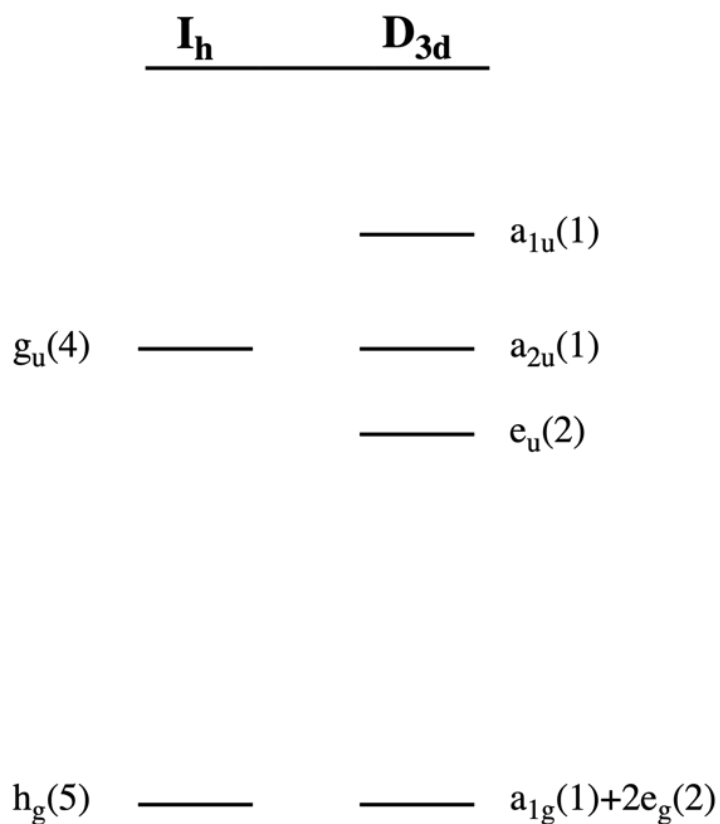


Figure 3.1. Hypoelectronic states are stabilized by a structural distortion, which lowers the overall energy of the cluster. The figure shows the *closo*-[B<sub>12</sub>]<sup>2-</sup> HOMO( $g_u$ ) and HOMO-1( $h_g$ ) on the left. Symmetry lowering to  $D_{3d}$  transforms  $g_u \rightarrow a_{1u}+a_{2u}+e_u$  and  $h_g \rightarrow a_{1g}+2e_g$ . Raising of the partially filled or unfilled  $a_{1u}$  and lowering the filled  $e_u$  is energetically favorable in hypoelectronic clusters.

### 3.2 Electrochemical Generation of $[B_{12}(OR)_{12}]^{1+}$

The anodic cyclic voltammogram of  $[B_{12}(OEt)_{12}]$  (**4**), collected in 0.2 M TBAPF<sub>6</sub> (tetrabutylammonium hexafluorophosphate) dichloromethane and acetonitrile electrolytes show two waves representing the known  $[4]^{1-/2-}$  and  $[4]^{1-/0}$  couples. The reduction potentials,  $E_{1/2}(1-/2-) = -1.08$  V and  $E_{1/2}(0/-1) = -0.454$  V in dichloromethane and  $E_{1/2}(1-/2-) = -0.94$  V and  $E_{1/2}(0/-1) = -0.41$  V in acetonitrile (all potentials reported versus the ferrocene-ferrocenium couple), are significantly less oxidizing than  $[B_{12}(OBz)_{12}]$  (Bz = CH<sub>2</sub>C<sub>6</sub>H<sub>5</sub>), which is the least oxidizing of the aryl-perfunctionalized clusters discussed in this thesis. Reported reduction potentials for  $[B_{12}(OBz)_{12}]$  in dichloromethane are  $E_{1/2}(1-/2-) = -0.7$  V and  $E_{1/2}(0/-1) = -0.2$  V, around 300 mV more positive than **4**.<sup>12,15</sup> The unusually negative reduction potentials of **4**, compared to other known  $[B_{12}(OR)_{12}]$  clusters, prompted us to explore the electrochemistry at highly oxidizing potentials. To our surprise, in dichloromethane, **4** shows a third reversible single-electron oxidation at  $E_{1/2} = 0.747$  V (Figure 3.2), which we assign to the  $[4]^{1+/0}$  couple. Cyclic voltammograms at scan rates between and 25–2500 mV/s were collected to explore the reversibility of the redox events. Figures 3.3–3.5 show individual cyclic voltammograms and plots of peak current ( $i_p$ ) as a function of the square root of the scan rate ( $v$ ); the linear relationship confirms the electrochemical reversibility of all three couples. Furthermore, Figure 3.6 shows a cyclic voltammogram displaying a strong irreversible wave at  $E_p = +1.3$  V. Comparison with a background scan collected for the 0.2 M TBAPF<sub>6</sub> dichloromethane electrolyte clearly shows that this wave involves **4**. We speculate that it corresponds to the  $[4]^{2+/1+}$  couple, and that  $[4]^{2+}$  partakes in rapid solvent or electrolyte oxidation reactions. In acetonitrile (Figure 3.7) neither of the  $[4]^{1-/2-}$  and  $[4]^{1-/0}$  waves are fully reversible and the  $[4]^{1+/0}$  couple appears completely irreversible. Table 3.1 summarizes the electrochemical data collected for **4** in

dichloromethane. Voltammograms collected in dichloromethane outside the glovebox, without pre-drying the solvent, show similar results. The reversibility of the waves were not negatively affected by the presence of water (see Section 3.5).

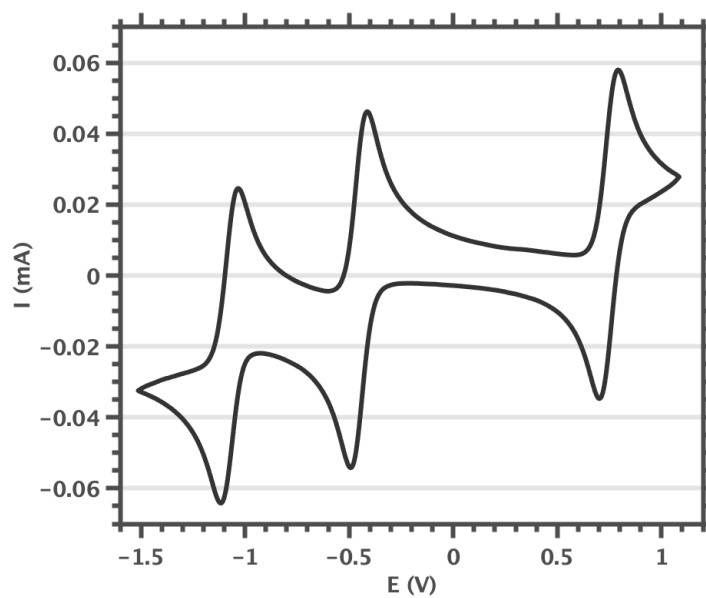


Figure 3.2. Cyclic voltammogram of 3.0 mM  $B_{12}(OEt)_{12}$  ( $4^0$ ) collected at 100 mV/s in 0.2 M TBAPF<sub>6</sub>/dichloromethane under air-free conditions. Potential reported versus the ferrocene-ferrocenium couple.

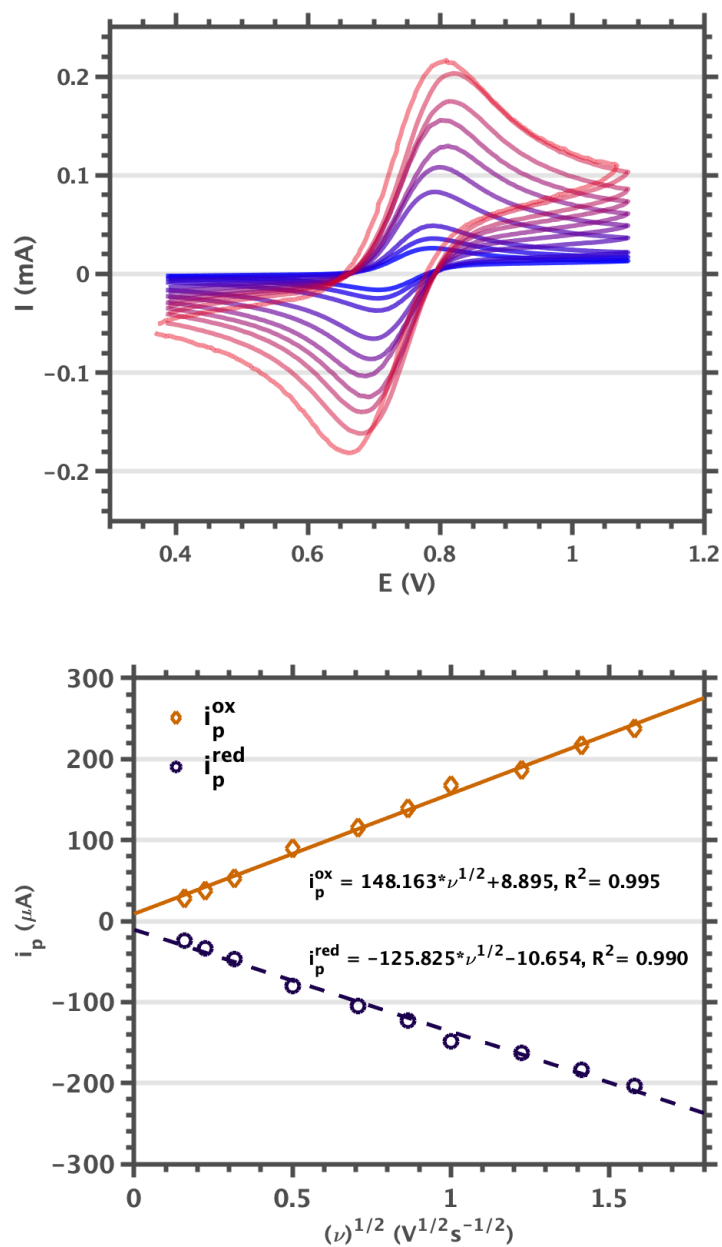


Figure 3.3. (Top) Cyclic voltammogram scan rate dependence of the  $[4]^{1+/0}$  couple. 3.0 mM  $4^0$  in 0.2 M TBAPF<sub>6</sub>/dichloromethane at 25 mV/s, 50 mV/s, 100 mV/s, 250 mV/s, 500 mV/s, 750 mV/s, 1000 mV/s, 1500 mV/s, 2000 mV/s and 2500 mV/s. (Bottom) Linear relationship between peak currents and scan rate.  $i_p^{\text{ox}}$  and  $i_p^{\text{red}}$  are the oxidative and reductive peak currents.  $\nu$  is the scan rate.

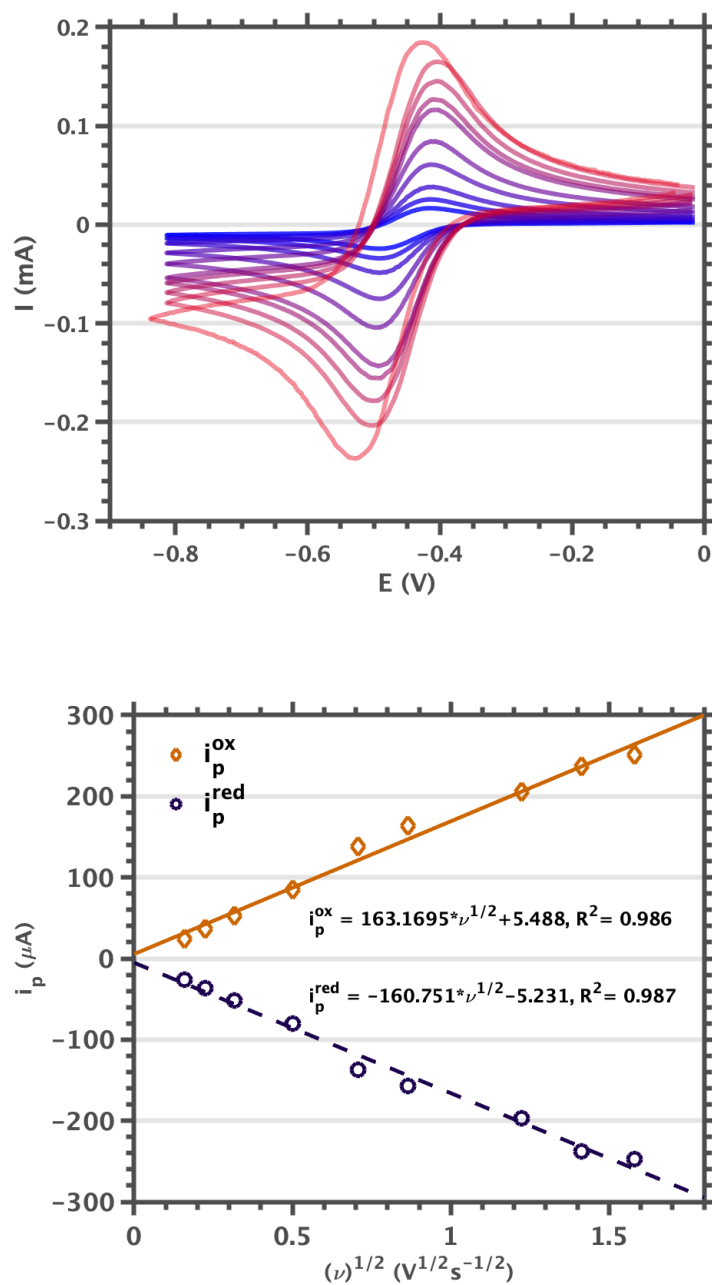


Figure 3.4. (Top) Cyclic voltammogram scan rate dependence of the  $[\mathbf{4}]^{0/1-}$  couple. 3.0 mM  $\mathbf{4}^0$  in 0.2 M TBAPF<sub>6</sub>/dichloromethane at 25 mV/s, 50 mV/s, 100 mV/s, 250 mV/s, 500 mV/s, 750 mV/s, 1000 mV/s, 1500 mV/s, 2000 mV/s and 2500 mV/s. (Bottom) Linear relationship between peak currents and scan rate.  $i_p^{\text{ox}}$  and  $i_p^{\text{red}}$  are the oxidative and reductive peak currents.  $\nu$  is the scan rate.

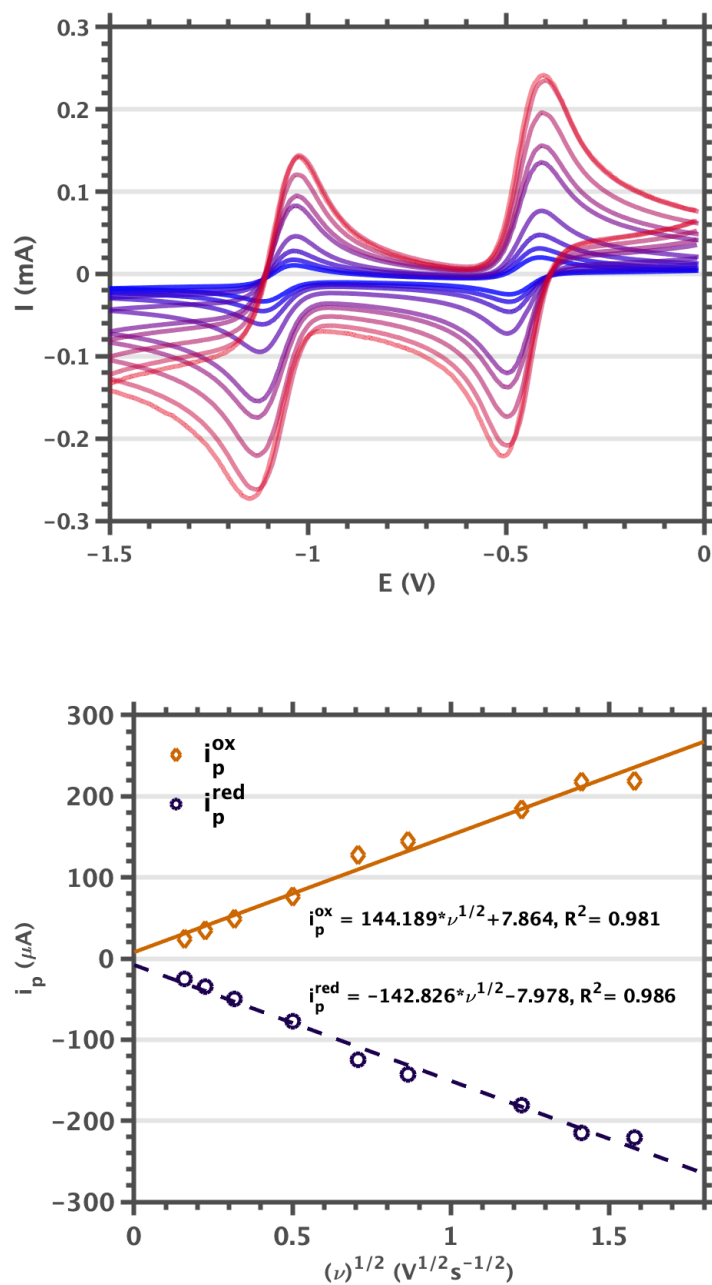


Figure 3.5. (Top) Cyclic voltammogram scan rate dependence of the  $[4]^{1-/2-}$  couple. 3.0 mM  $4^0$  in 0.2 M TBAPF<sub>6</sub>/dichloromethane at 25 mV/s, 50 mV/s, 100 mV/s, 250 mV/s, 500 mV/s, 750 mV/s, 1000 mV/s, 1500 mV/s, 2000 mV/s and 2500 mV/s. (Bottom) Linear relationship between peak currents and scan rate.  $i_p^{\text{ox}}$  and  $i_p^{\text{red}}$  are the oxidative and reductive peak currents.  $\nu$  is the scan rate. The voltammogram was collected starting from  $4^0$ .

Table 3.1. (cont. next page) Electrochemical parameters for 3.0 mM  $4^0$  in 0.2 M TBAPF<sub>6</sub>/dichloromethane.  $E_{p}^{ox}$  and  $E_{p}^{red}$  are the potentials at peak current for the respective oxidative and reductive waves.  $E_{1/2}$  is the mean of the reductive and oxidative peak potential.  $i_p^{ox}$  and  $i_p^{red}$  are the peak currents observed at the absolute maximum of the respective oxidative and reductive waves. All potentials are reported versus the ferrocene-ferrocenium couple.

Couple	$v$	25 mV/s	50 mV/s	100 mV/s	250 mV/s	500 mV/s
[4] <sup>1-/2-</sup>	$E_{1/2}$ (V)	-1.072	-1.075	-1.075	-1.079	-1.085
	$E_p^{ox}$ (V)	-1.030	-1.038	-1.037	-1.034	-1.038
	$E_p^{red}$ (V)	-1.114	-1.113	-1.113	-1.125	-1.133
	$i_p^{ox}$ ( $\mu$ A)	+24.67	+34.29	+49.15	+76.72	+127.7
	$i_p^{red}$ ( $\mu$ A)	-24.90	-34.51	-49.50	-77.71	-124.6
[4] <sup>0/1-</sup>	$E_{1/2}$ (V)	-0.452	-0.452	-0.454	-0.454	-0.454
	$E_p^{ox}$ (V)	-0.414	-0.414	-0.418	-0.410	-0.410
	$E_p^{red}$ (V)	-0.490	-0.490	-0.490	-0.498	-0.498
	$i_p^{ox}$ ( $\mu$ A)	+24.21	+36.51	+52.57	+84.83	+138.3
	$i_p^{red}$ ( $\mu$ A)	-25.77	-36.55	-52.11	-80.48	-137.2
[4] <sup>1+/0</sup>	$E_{1/2}$ (mV)	+0.747	+0.749	+0.747	+0.747	+0.749
	$E_p^{ox}$ (mV)	+0.785	+0.789	+0.785	+0.793	+0.797
	$E_p^{red}$ (mV)	+0.709	+0.709	+0.709	+0.701	+0.701
	$i_p^{ox}$ ( $\mu$ A)	+28.22	+37.50	+52.82	+90.00	+115.7
	$i_p^{red}$ ( $\mu$ A)	-24.24	-33.51	-47.34	-80.64	-105.1

Couple	v	750 mV/s	1000 mV/s	1500 mV/s	2000 mV/s	2500 mV/s
[4] <sup>1-/2-</sup>	E <sub>1/2</sub> (V)	-1.083	-	-1.080	-1.081	-1.091
	E <sub>p</sub> <sup>ox</sup> (V)	-1.030	-	-1.030	-1.022	-1.027
	E <sub>p</sub> <sup>red</sup> (V)	-1.137	-	-1.129	-1.141	-1.155
	i <sub>p</sub> <sup>ox</sup> (μA)	+145.1	-	+184.0	+218.2	+219.0
	i <sub>p</sub> <sup>red</sup> (μA)	-143.1	-	-180.4	-215.2	-220.4
[4] <sup>0/1-</sup>	E <sub>1/2</sub> (V)	-0.452	-	-0.454	-0.450	-0.456
	E <sub>p</sub> <sup>ox</sup> (V)	-0.410	-	-0.410	-0.402	-0.404
	E <sub>p</sub> <sup>red</sup> (V)	-0.494	-	-0.498	-0.497	-0.508
	i <sub>p</sub> <sup>ox</sup> (μA)	+163.6	-	+205.5	+236.8	+251.5
	i <sub>p</sub> <sup>red</sup> (μA)	-156.7	-	-197	-237.5	-247.6
[4] <sup>1+/0</sup>	E <sub>1/2</sub> (mV)	+0.751	+0.747	+0.751	+0.757	+0.742
	E <sub>p</sub> <sup>ox</sup> (mV)	+0.813	+0.801	+0.813	+0.825	+0.813
	E <sub>p</sub> <sup>red</sup> (mV)	+0.689	+0.693	+0.689	+0.689	+0.672
	i <sub>p</sub> <sup>ox</sup> (μA)	+139.2	+167.9	+186.9	+217.3	+237.4
	i <sub>p</sub> <sup>red</sup> (μA)	-122.6	-148.6	-162.6	-184	203.4

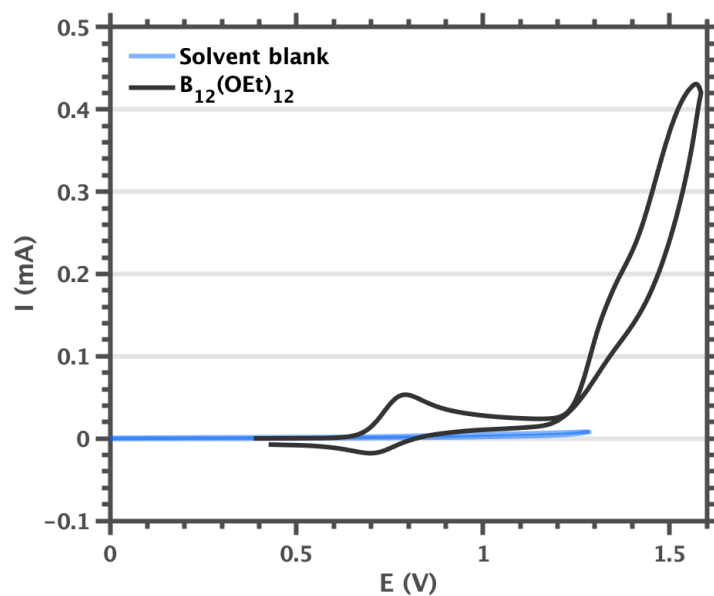


Figure 3.6. (Black trace) Cyclic voltammogram of 3.0 mM  $4^0$  collected at 100 mV/s in 0.2 M TBAPF<sub>6</sub>/dichloromethane under air-free conditions. (Blue trace) Electrolyte background scan. Potential reported versus the ferrocene-ferrocenium couple.

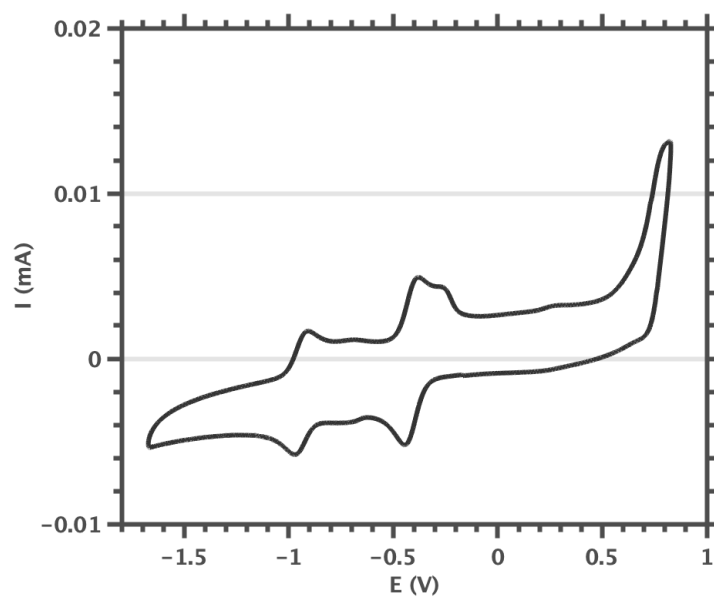


Figure 3.7. Cyclic voltammogram of 3.0 mM  $4^0$  collected at 100 mV/s in 0.2 M TBAPF<sub>6</sub>/acetonitrile. Potential reported versus the ferrocene-ferrocenium couple.

Spectroelectrochemical characterization was performed to further probe the identity of the super-oxidized species. In a 0.1 M TBAPF<sub>6</sub> dichloromethane solution we were able to generate [4]<sup>1+</sup> by holding the potential at +1.2 V. Figure 3.8 shows spectra collected while holding the potential at (A) -0.5 V, (B) -1 V and (C) +1.2 V (after holding at +0.8 V to recover 4<sup>0</sup>). The strong visible absorption band of 4<sup>0</sup> at 460 nm blue-shifts very slightly to 455 nm upon oxidation to [4]<sup>1+</sup>. Interestingly, [4]<sup>1+</sup> shows an additional broad lower-energy absorption band centered at 700 nm. Under the given conditions, [4]<sup>1+</sup> persists under applied bias but the visible spectrum indicates rapid reversible recovery of 4<sup>0</sup> when no potential is applied. Although significant non-coulombic currents were passed, the observed spectra indicate that we were able to reversibly cycle through all four oxidation states (2-/1-/0/1+). The spectral reversibility support assigning the super-oxidized species to [4]<sup>1+</sup>. The non-coulombic currents likely stem from solvent oxidation or oxidation of adventitious water.

### 3.3 Chemical Generation of [B<sub>12</sub>(OR)<sub>12</sub>]<sup>1+</sup>

Following our initial electrochemical and spectroelectrochemical observation of [4]<sup>1+</sup>, we wanted to attempt isolating [4]<sup>1+</sup> through chemical means. A range of chemical oxidants were explored, including silver triflate, nitrosonium tetrafluoroborate, tungsten hexachloride and Magic Blue (tris(4-bromophenyl)ammoniumyl hexachloroantimonate). Only treatment with Magic Blue resulted in observable reactivity. Addition of Magic Blue to tetrahydrofuran (THF), dichloromethane and nitromethane solutions of 4<sup>0</sup> resulted in rapid consumption of the dark blue Magic Blue radical.<sup>21</sup> Visually observed color shifts suggested that [4]<sup>1+</sup> had been generated, but the species was too short-lived for spectroscopic characterization.

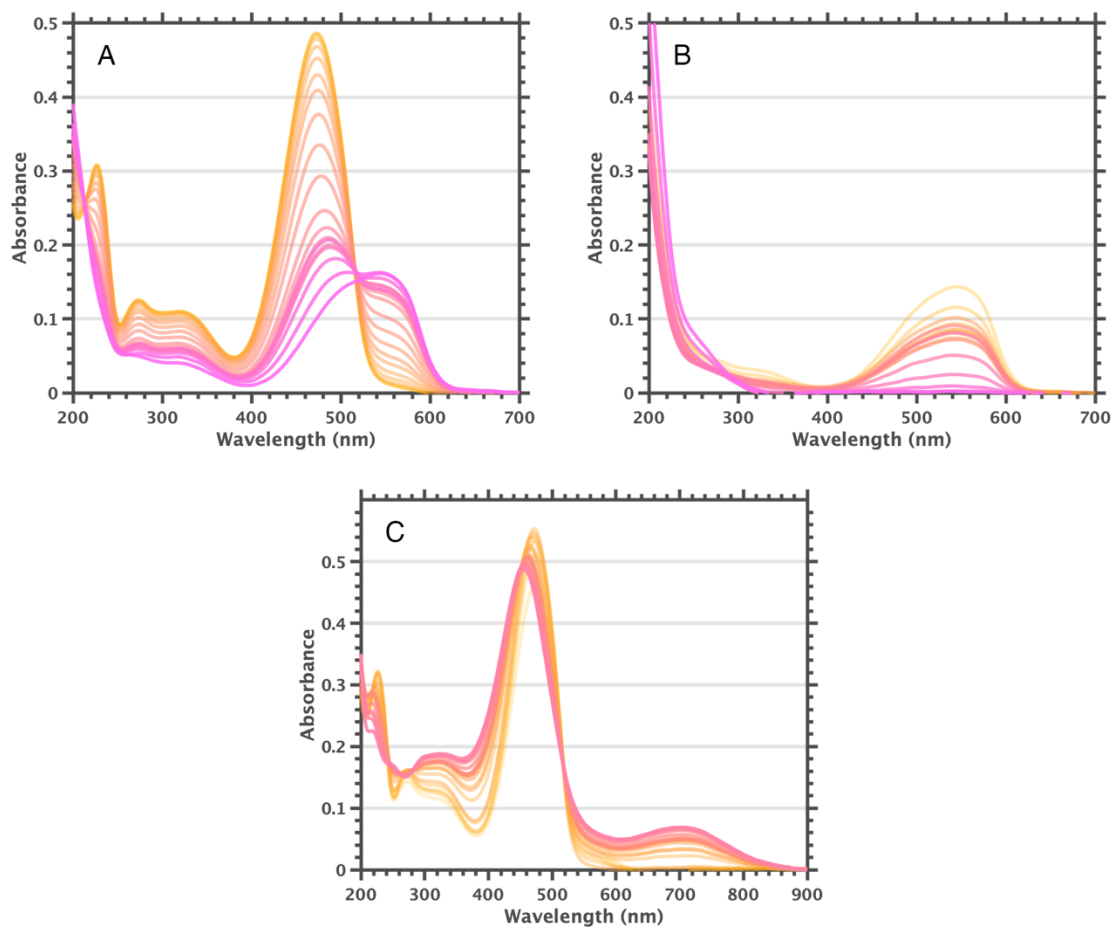


Figure 3.8 Electrochemically derived spectra of **4** in 0.1 M TBAPF<sub>6</sub>/CH<sub>2</sub>Cl<sub>2</sub>. (A) Potential held at -0.5 V to generate [4]<sup>1+</sup>. (B) Potential held at -1 V to generate [4]<sup>2-</sup>. (C) Potential held at +1.2 V to generate [4]<sup>1+</sup>. (**4**<sup>0</sup> was first regenerated from [4]<sup>2-</sup> by holding the potential at +0.8 V). Potentials reported versus the ferrocene-ferrocenium couple.

Titration of a THF solution of  $\mathbf{4}^0$  (60  $\mu\text{M}$ ) with Magic Blue, monitored by UV-visible spectroscopy, provided suggestive evidence of oxidation to  $[\mathbf{4}]^{1+}$  followed by rapid solvent oxidation. Figure 3.9 shows UV-visible spectra taken after addition of 25  $\mu\text{l}$  aliquots of a 0.64 mM solution of Magic Blue in THF. A total of 250  $\mu\text{l}$  was added, yielding a 37.5  $\mu\text{M}$  final concentration. The strong band growing in at 310 nm is indicative of the formation of neutral tris(4-bromophenyl)amine, suggesting that the oxidant had been consumed. The absence of the strong absorption bands characteristic of Magic Blue further confirmed that the oxidant had been consumed. Solutions of Magic Blue in THF without  $\mathbf{4}^0$  last for hours without appreciable consumption of the oxidant, implying that  $[\mathbf{4}]^{1+}$  plays a key role. Furthermore, this data suggests that  $[\mathbf{4}]^{1+}$  act as an oxidation catalyst, given that no consumption of  $\mathbf{4}^0$  is observed.

It is noteworthy that  $[\mathbf{4}]^{1+}$  appears to be a potent catalyst, based on the electrochemical observations in acetonitrile and dichloromethane, as well as the suggested oxidation of solvent occurring after chemical oxidation of  $\mathbf{4}^0$ . In the case of Magic Blue, in addition to solvent oxidation, there is evidence that chemical transformations involving Magic Blue or the tris(4-bromophenyl)amine product may occur following formation of  $[\mathbf{4}]^{1+}$ . A crystal structure grown out of a solution of  $\mathbf{4}^0$  and Magic Blue in dichloromethane shows the presence of a tris(4-bromophenyl)amine or tris(4-bromophenyl)ammoniumyl species with partial 2-bromination (Figure 3.8). Due to poor crystal quality we cannot derive reliable bond lengths, which prohibit differentiation of the amine and ammoniumyl radicals. We do not yet understand what causes 2-bromination, but postulate that  $[\mathbf{4}]^{1+}$  is involved in bromine transfer reactivity. That said, only a single small crystal was obtained containing the 2-brominated phenylamine, which could mean

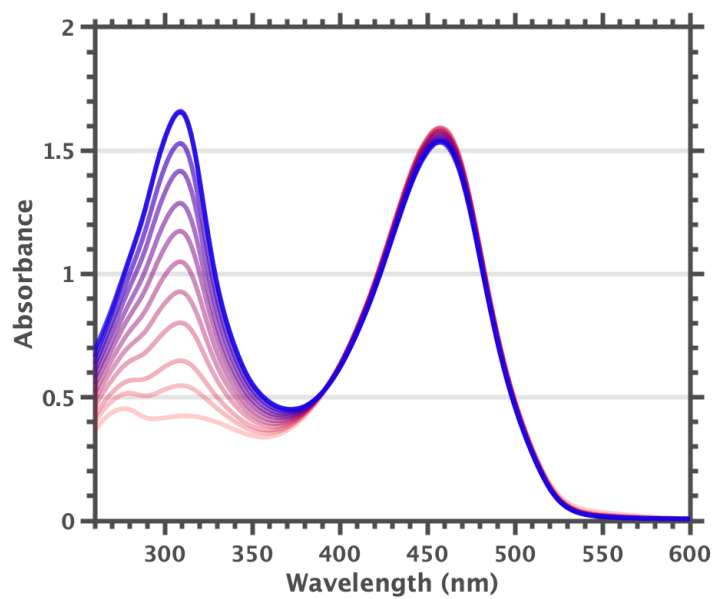


Figure 3.9: Spectrum of 60  $\mu\text{M}$   $4^0$  in THF titrated with a 0.64 mM solution of Magic Blue in THF. Each data point corresponds to a 25  $\mu\text{l}$  addition of Magic Blue solution. A slight decrease in the 460 nm band is observed due to sample dilution.

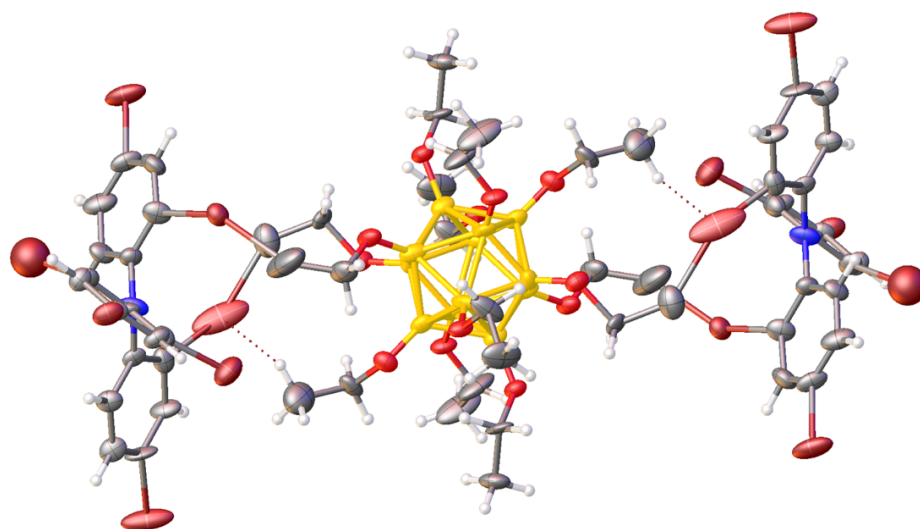


Figure 3.10: Crystal structure showing the unusual 2-bromianted phenyl groups of triphenylamines/ammoniumyls surrounding [4].

that it is only a minor side product. It is also plausible that commercial Magic Blue contains trace amounts of 2-brominated contaminants, which could be either in the ammoniumyl radical form or the uncharged amine form. A number of other crystals were collected from the sample, all displaying unit cells analogous to the known structure of **4**<sup>0</sup>.

Based on the observations presented above, we hypothesized that Magic Blue is able to oxidize **4**<sup>0</sup>, but not sufficiently strong of an oxidant to enable isolation of a [**4**]<sup>1+</sup> salt. We wondered if a more oxidizing ammoniumyl radical, such as tris(2,4-dibromophenyl)ammoniumyl hexachloroantimonate (henceforth referred to as Magic Green) would be more successful. The redox potential of Magic Blue is around +0.70 mV. 2-bromination provides Magic Green with an additional 440 mV of oxidizing power, bringing its redox potential to +1.14 mV (versus the ferrocene-ferrocenium couple).<sup>22</sup> Given that Magic Green is not commercially available and that the highly reactive nature of the reagents involved in synthesis demand expertise beyond our abilities, we asked for assistance from the Spokoyny lab.

We were excited to learn that using in-house prepared Magic Green, members of the Spokoyny lab had been able to isolate [B<sub>12</sub>(OC<sub>2</sub>H<sub>4</sub><sup>i</sup>Pr)<sub>12</sub>]<sup>1+</sup> ([**5**]<sup>1+</sup>) as a hexachloroantimonate salt. The salt had to be handled under rigorously dry and air-free conditions at all times and, even then, it decomposes over time (weeks). So far, [**5**][SbCl<sub>6</sub>] salts of sufficient purity for spectroscopic characterization have not been obtained. However, we were able to collect electronic paramagnetic resonance (EPR) data on *in-situ* prepared [**4**]<sup>1+</sup> and [**5**]<sup>1+</sup>. Both X-band continuous wave (CW) EPR spectra and pulsed Q-band ESE-EPR, HYSCORE and ENDOR spectra were collected on samples prepared by adding a substoichiometric amount of Magic Green to toluene solutions of **4**<sup>0</sup> and toluene/dichloromethane-*d*<sub>2</sub> solutions of **5**<sup>0</sup>. The CW EPR spectrum of [**5**]<sup>1+</sup>,

shown in Figure 3.11, displays a broad unresolved signal around  $g = 2.0083$ , highly reminiscent of the monoanionic species previously described in the literature (*vide supra*). This indicates that the SOMO of  $[\text{B}_{12}]^{1+}$  is highly delocalized, similar to what has been suggested for the SOMO of *hypocloso*- $[\text{B}_{12}]^{1-}$ , and further validates our assignment of the super-oxidized species as  $[\text{B}_{12}]^{1+}$ . Additional EPR data and an in-depth analysis of the results can be found in Chapter 4.

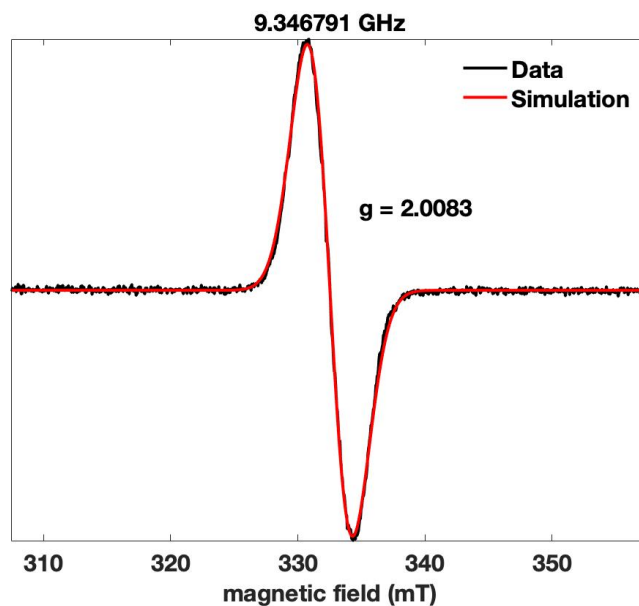


Figure 3.11. X-band CW EPR spectrum of  $[\text{5}]^{1+}$  in toluene glass at 77 K. The cation was in-situ generated by reaction with a substoichiometric amount of Magic Green.

### 3.4 Conclusions

We have shown that super-oxidized  $[\text{B}_{12}(\text{OR})_{12}]^{1+}$  (R = alkyl) species can be reversibly generated through electrochemical methods. Additionally, collaborators in the Spokoyny lab have been able to isolate  $[\mathbf{5}][\text{SbCl}_6]$  using the strong ammoniumyl radical oxidant (Magic Green). The discovery of these super-oxidized dodecaborates is a significant breakthrough, as it was previously believed that depopulation of the *hypercloso*- $\text{B}_{12}^0$  HOMO( $a_{2u}$ ) would lead to cluster decomposition. This also poses questions around what kind of reactivities these super-oxidized species can access, and, if even higher oxidation states can be isolated in clusters carrying sufficiently electron-donating substituents. These questions are stimulated by preliminary indications suggesting that  $[\mathbf{4}]^{1+}$  partake in catalytic oxidation reactions and that a  $[\mathbf{4}]^{2+}$  species can be electrochemically generated in dichloromethane. Further studies are currently underway to systematically describe the electrochemical, chemical and spectroscopic properties of  $[\text{B}_{12}(\text{OR})_{12}]^{1+}$  clusters.

### 3.5 Experimental Details

#### Compounds

$4^0$ ,  $5^0$ ,  $[5][SbCl_6]$  and Magic Green were obtained from the Spokoyny lab.

#### Electrochemistry

##### *Air-free electrochemistry*

All sample preparation and measurements were performed inside an argon-filled glove box, which had been equipped with BNC ports to enable connection of an external potentiostat. Cyclic voltammograms were collected on a Gamry Reference 600 potentiostat using a small-volume electrochemical cell. Electrochemical grade TBAPF<sub>6</sub> (Sigma-Aldrich) had been previously recrystallized from hot ethanol and dried under vacuum. A  $d = 3.0$  mm glassy carbon working electrode (BASi), a Pt wire counter-electrode and an Ag/AgCl reference electrode was used (BASi). The reference was prepared by placing a polished silver wire in a 0.01 M AgNO<sub>3</sub>/0.2 M TBAPF<sub>6</sub> acetonitrile solution. A CoralPor (BASi) frit provided electrochemical contact between the reference solution and sample solution.

Dichloromethane (Millipore) and acetonitrile (Millipore) had been dried for > 84 hours over activated 3 Å molecular sieves (Sigma-Aldrich). After drying, the solvents were distilled and degassed through multiple freeze-pump-thaw cycles. Sample solutions were prepared at approximately 3.0 mM  $4^0$  in 0.2 M TBAPF<sub>6</sub> electrolyte. Between each measurement the sample solution was thoroughly mixed, and the working electrode was polished with a Kimwipe (Kimtech) to remove any residue formed during preceding cycles. A speck of ferrocene (Sigma-Aldrich, purified through sublimation) was added after the final measurement and a cyclic voltammogram was collected at a 100 mV/s. The ferrocene/ferrocenium wave was used as the reference.

The EC-Lab software package (Biologic) was used to analyze the data. Electrochemical parameters were obtained using the Wave Analysis function, taking care to select appropriate baselines. 100 mV/s scans were used to extract final  $E_p$  values. The parameters presented in Table 2.1 were derived from the individual wave data shown in Figure (3.3–3.5).

#### *Open-air electrochemistry*

Open-air experiments were performed using a CH Instruments potentiostat. Solutions were prepared at  $\sim 2$  mM  $4^0$  in 0.1 M TBAPF<sub>6</sub> dichloromethane (Millipore, used as received) electrolyte. A small-volume electrochemical cell was used for all experiments (BASi). Electrochemical grade TBAPF<sub>6</sub> (Sigma-Aldrich) had been previously recrystallized from hot ethanol and dried rigorously under vacuum. A  $d = 3.0$  mm glassy carbon working electrode (BASi), a Pt wire counter-electrode and an Ag/AgCl reference electrode was used (BASi). The reference was prepared by placing a polished silver wire in a 0.01 M AgNO<sub>3</sub>/0.1 M TBAPF<sub>6</sub> acetonitrile solution. A CoralPor (BASi) frit provided electrochemical contact between the reference solution and sample solution.

The sample solution was degassed by argon bubbling both before the initial measurement. The gas had first been saturated with dichloromethane by passing it through a bubbler containing dry solvent and activated 3 Å molecular sieves (Sigma-Aldrich). Between each measurement the sample solution was thoroughly mixed by argon bubbling and the working electrode was polished on a polishing pad (BASi). After the final measurement a speck of ferrocene (Sigma-Aldrich, purified through sublimation) was added. A cyclic voltammogram was collected at a 100 mV/s and the ferrocene/ferrocenium wave was used as the reference. The MATLAB software package (Mathworks) was used to analyze the data. Electrochemical parameters were

obtained using a custom made scripts, taking care to select appropriate baselines. Cyclic voltammograms collected between 25 and 500 mV/s are shown in Figure 3.12. Figure 3.13–3.15 show plots of peak potential ( $i_p$ ) as a function of the square root of scan rate ( $v$ ). The linear relationships confirm the reversibility of all three couples.

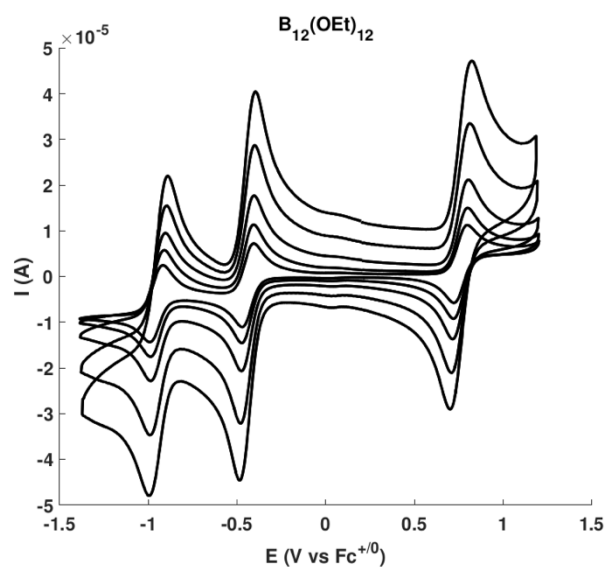


Figure 3.12: Cyclic voltammogram scan rate dependence.  $\sim 2\text{mM}$  ( $4^0$ ) in  $0.1\text{ M TBAPF}_6/\text{dichloromethane}$  at  $25\text{ mV/s}$ ,  $50\text{ mV/s}$ ,  $100\text{ mV/s}$ ,  $250\text{ mV/s}$  and  $500\text{ mV/s}$ .

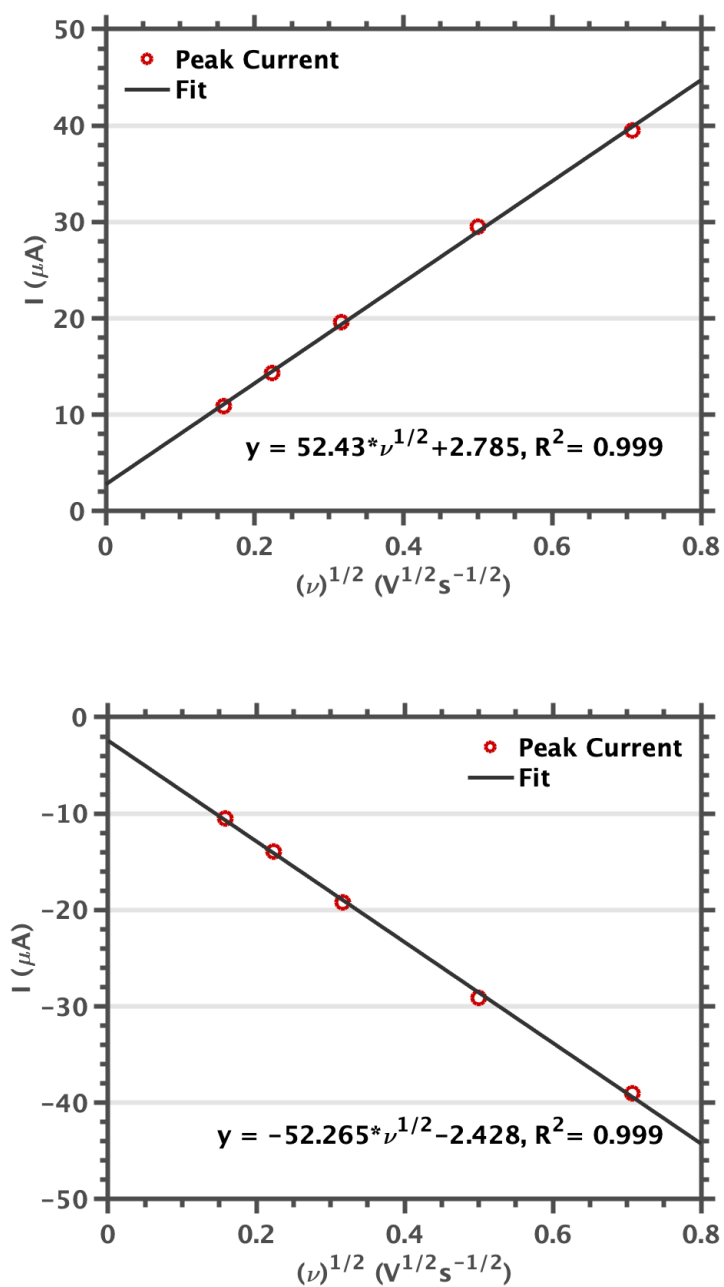


Figure 3.4.  $I_p$  vs  $(\nu)^{1/2}$  plots for the  $[4]^{1-/2-}$  couple. The top figure shows peak potentials observed for oxidation of  $[4]^{2-}$  to  $[4]^{1-}$  while the bottom figure shown peak potentials observed of reduction of  $[4]^{1-}$  to  $[4]^{2-}$ .

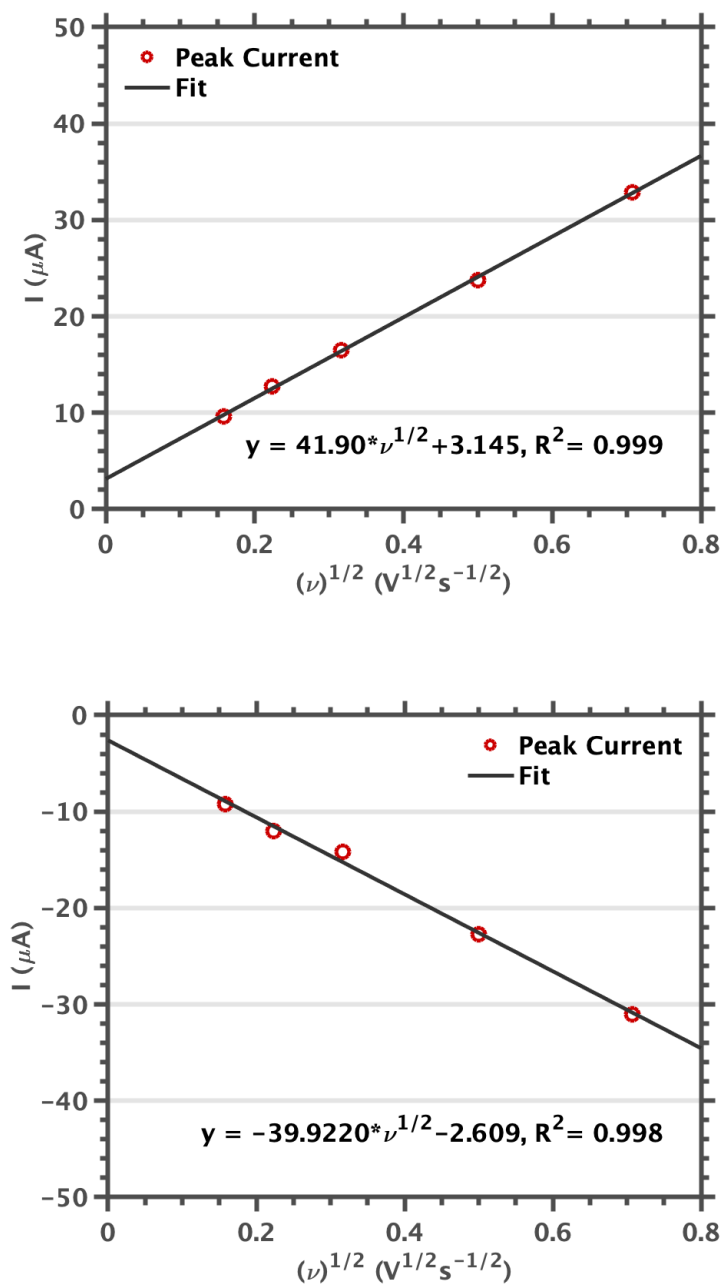


Figure 3.5.  $I_p$  vs  $(\nu)^{1/2}$  plots for the  $[4]^{0/1-}$  couple. The top figure shows peak potentials observed for oxidation of  $[4]^{1-}$  to  $4^0$  while the bottom figure shown peak potentials observed of reduction of  $4^0$  to  $[4]^{1-}$ .

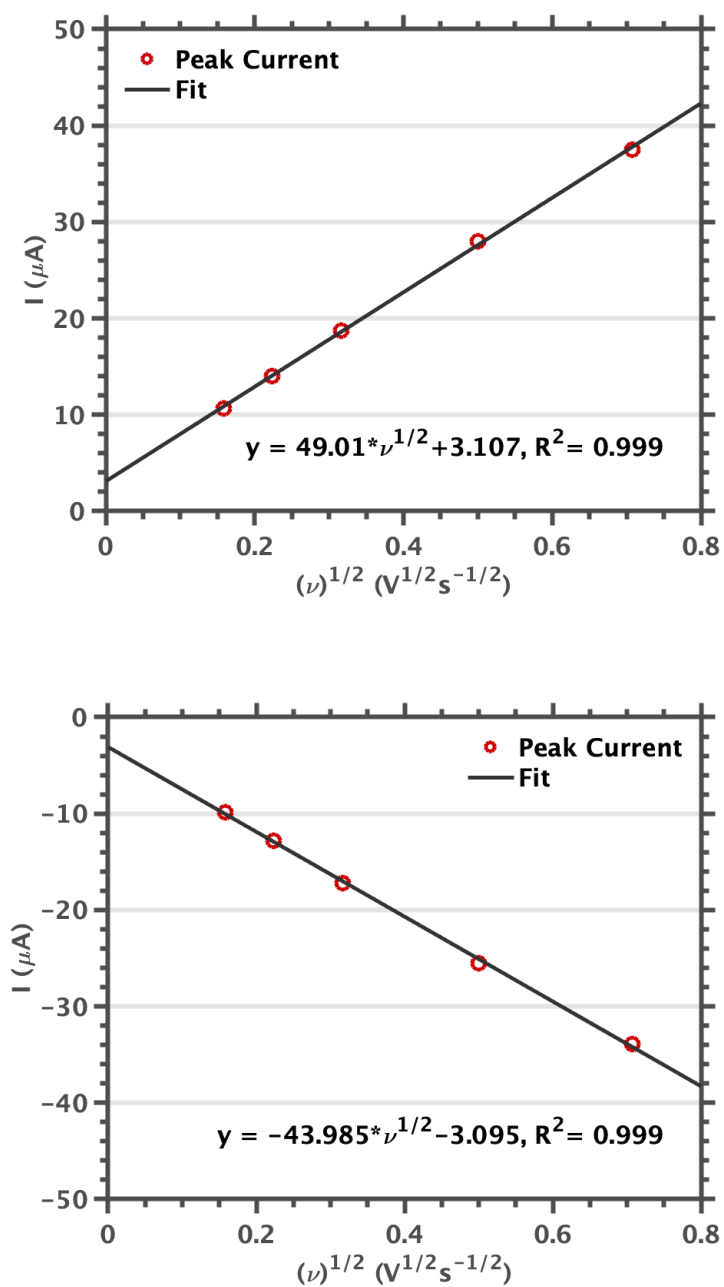


Figure 3.6.  $I_p$  vs  $(\nu)^{1/2}$  plots for the  $[4]^{1+/0}$  couple. The top figure shows peak potentials observed for oxidation of  $4^0$  to  $[4]^{1+}$  while the bottom figure shown peak potentials observed of reduction of  $[4]^{1+}$  to  $4^0$ .

### **Spectroelectrochemistry**

Solution preparation and control cyclic voltammograms were performed as described above (open-air electrochemistry), with the modification that the  $4^0$  concentration was optimized for spectroelectrochemistry. A portable Pine WaveNow potentiostat was used to provide applied bias, while a Varian Cary 50 Bio UV-visible spectrometer was used to collect spectra. Data was collected using a 0.5 mm path length quartz spectroelectrochemical cell (BASi) and a gold mesh working electrode (BASi). Each potential was held until complete conversion to the desired oxidation state was apparent in the UV-visible spectrum. Due to the design of the spectroelectrochemistry cell, although attempts were made to keep the solution under argon at all times, we cannot guarantee rigorously air-free conditions.

### **Chemical oxidation**

Reactivity was monitored by visual observations and UV-visible spectra collected on a Varian Cary 50 Bio UV-visible spectrometer. All experiments were performed under air-free conditions. Samples were prepared in Schlenk cuvettes to facilitate collection of UV-visible spectra without compromising the samples.

### *Solvents*

3 Å Molecular sieves (Sigma-Aldrich) had been activated through heating to 180°C under dynamic vacuum for > 12 hours. Activated sieves were stored under vacuum and the storage vessel was placed under positive argon pressure when sieves were being transferred to solvent drying vessels. Before addition of solvent, the solvent vessels and sieves were flame dried.

Nitromethane (Sigma-Aldrich) was dried for > 48 hours over activated 3 Å molecular sieves, followed by three > 30 minute freeze-pump-thaw cycles. Finally, the solvent was allowed to

stand over sieves for an additional > 24 hours. An analogous procedure was applied to dry dichloromethane (Millipore). Tetrahydrofuran (Millipore) had been pre-dried on a commercial solvent purification system. The solvent was transferred to a Strauss flask and degassed through multiple freeze-pump-thaw cycles. The flask was then transferred into a nitrogen-filled glove box and the solvent further dried through stirring over NaK.

*Nitrosonium tetrafluoroborate*

A small speck of nitrosonium tetrafluoroborate (Sigma-Aldrich) was added to solutions of  $4^0$  in nitromethane, tetrahydrofuran and dichloromethane. No reactivity was observed.

*Silver triflate*

Solid silver triflate (Sigma-Aldrich) was added to solutions of  $4^0$  in nitromethane and dichloromethane. The UV-visible spectrum of the solution was monitored over hours. No reactivity was observed.

*Magic Blue*— $[(4\text{-Br-C}_6\text{H}_4)_3\text{N}]\text{SbCl}_6$

A solution of  $4^0$  in tetrahydrofuran and dichloromethane was prepared. A speck of Magic Blue (Sigma-Aldrich) was added. The solution immediately turned green but over minutes converted to a dark brown color, in line with what we expect for  $[4]^{1+}$ .

A follow-up experiment was performed by titrating a 0.060 mM solution of  $4^0$  in tetrahydrofuran with a 0.64 mM solution of Magic Blue in tetrahydrofuran. 25  $\mu\text{l}$  microliter additions were made. UV-visible spectra were collected after each addition, first allowing the sample to equilibrate. A total of 250  $\mu\text{l}$  Magic Blue solution was added, yielding a final concentration 0.0365 mM

### **X-band CW Electronic Paramagnetic Resonance of [5]<sup>1+</sup>**

All manipulations were carried out inside a nitrogen-filled glove box. Samples were placed in X-band EPR tubes equipped with a J. Young valve and froze in liquid nitrogen immediately after removal from the glove box. Toluene (Millipore) had been dried on a commercial solvent purification system, followed by distillation and multiple freeze-pump-thaw cycles before transferring the solvent into the glove box. Inside the glove box, the solvent was stored over activated 3 Å molecular sieves (Sigma-Aldrich). Samples were prepared by dissolving 1.7 mg Magic Green and 3 mg **5**<sup>0</sup> in 1 ml toluene. An aliquot of solution was transferred to the EPR tube, which was immediately sealed, removed from the glove box and frozen in liquid nitrogen.

X-band EPR spectra were obtained on a Bruker EMX spectrometer at 77 K in a liquid nitrogen dewar using Bruker Win-EPR software (ver. 3.0). Spectra were collected over a 1–8 mW power range, and 5 scans were averaged for each spectrum. Spectral simulation was performed using the EasySpin<sup>23</sup> Simulation toolbox with MATLAB 2019a .

## BIBLIOGRAPHY

- (1) Longuet-Higgins, H. C.; Roberts, M. D. V. The Electronic Structure of an Icosahedron of Boron Atoms. *Proc R Soc Lond A* **1955**, *230* (1180), 110–119. <https://doi.org/10.1098/rspa.1955.0115>.
- (2) Lipscomb, W. N. Recent Studies of the Boron Hydrides. In *Advances in Inorganic Chemistry and Radiochemistry*; Emeléus, H. J., Sharpe, A. G., Eds.; Academic Press, 1959; Vol. 1, pp 117–156. [https://doi.org/10.1016/S0065-2792\(08\)60253-8](https://doi.org/10.1016/S0065-2792(08)60253-8).
- (3) Lipscomb, W. N.; Britton, D. Valence Structure of the Higher Borides. *J. Chem. Phys.* **1960**, *33* (1), 275–280. <https://doi.org/10.1063/1.1731097>.
- (4) Hoffmann, R.; Lipscomb, W. N. Theory of Polyhedral Molecules. I. Physical Factorizations of the Secular Equation. *J. Chem. Phys.* **1962**, *36* (8), 2179–2189. <https://doi.org/10.1063/1.1732849>.
- (5) Hoffmann, R.; Lipscomb, W. N. Boron Hydrides: LCAO—MO and Resonance Studies. *J. Chem. Phys.* **1962**, *37* (12), 2872–2883. <https://doi.org/10.1063/1.1733113>.
- (6) Moore, E. B.; Lohr, L. L.; Lipscomb, W. N. Molecular Orbitals in Some Boron Compounds. *J. Chem. Phys.* **1961**, *35* (4), 1329–1334. <https://doi.org/10.1063/1.1732046>.
- (7) Eberhardt, W. H.; Crawford, B.; Lipscomb, W. N. The Valence Structure of the Boron Hydrides. *J. Chem. Phys.* **1954**, *22* (6), 989–1001. <https://doi.org/10.1063/1.1740320>.
- (8) Wiersema, R. J.; Middaugh, R. L. Electrochemical Preparation and Halogenation of 1,1'- $\mu$ -Hydro-Bis(Undecahydro-Closo-Dodecaborate)(3-), B<sub>24</sub>H<sub>233</sub>-. *Inorg. Chem.* **1969**, *8* (10), 2074–2079. <https://doi.org/10.1021/ic50080a009>.
- (9) Wade, K. The Structural Significance of the Number of Skeletal Bonding Electron-Pairs in Carboranes, the Higher Boranes and Borane Anions, and Various Transition-Metal Carbonyl Cluster Compounds. *J. Chem. Soc. Chem. Commun.* **1971**, No. 15, 792–793. <https://doi.org/10.1039/C29710000792>.
- (10) J. Welch, A. The Significance and Impact of Wade's Rules. *Chem. Commun.* **2013**, *49* (35), 3615–3616. <https://doi.org/10.1039/C3CC00069A>.
- (11) Peymann, T.; Knobler, C. B.; Hawthorne, M. F. An Unpaired Electron Incarcerated within an Icosahedral Borane Cage: Synthesis and Crystal Structure of the Blue, Air-Stable {[Closo-B<sub>12</sub>(CH<sub>3</sub>)<sub>12</sub>]·}– Radical. *Chem. Commun.* **1999**, *0* (20), 2039–2040. <https://doi.org/10.1039/A905406E>.

- (12) Peymann, T.; Knobler, C. B.; Khan, S. I.; Hawthorne, M. F. Dodeca(Benzyloxy)Dodecaborane, B12(OCH2Ph)12: A Stable Derivative of Hypercloso-B12H12. *Angew. Chem. Int. Ed.* **2001**, *40* (9), 1664–1667. [https://doi.org/10.1002/1521-3773\(20010504\)40:9<1664::AID-ANIE16640>3.0.CO;2-O](https://doi.org/10.1002/1521-3773(20010504)40:9<1664::AID-ANIE16640>3.0.CO;2-O).
- (13) Van, N.; Tiritiris, I.; Winter, R. F.; Sarkar, B.; Singh, P.; Duboc, C.; Muñoz-Castro, A.; Arratia-Pérez, R.; Kaim, W.; Schleid, T. Oxidative Perhydroxylation of [Closo-B12H12]2− to the Stable Inorganic Cluster Redox System [B12(OH)12]2−/−: Experiment and Theory. *Chem. – Eur. J.* **2010**, *16* (37), 11242–11245. <https://doi.org/10.1002/chem.201001374>.
- (14) Boéré, R. T.; Derendorf, J.; Jenne, C.; Kacprzak, S.; Keßler, M.; Riebau, R.; Riedel, S.; Roemmele, T. L.; Rühle, M.; Scherer, H.; et al. On the Oxidation of the Three-Dimensional Aromatics [B12X12]2− (X=F, Cl, Br, I). *Chem. – Eur. J.* **2014**, *20* (15), 4447–4459. <https://doi.org/10.1002/chem.201304405>.
- (15) Wixtrom, A. I.; Shao, Y.; Jung, D.; Machan, C. W.; Kevork, S. N.; Qian, E. A.; Axtell, J. C.; Khan, S. I.; Kubiak, C. P.; Spokoyny, A. M. Rapid Synthesis of Redox-Active Dodecaborane B12(OR)12 Clusters under Ambient Conditions. *Inorg. Chem. Front.* **2016**, *3* (5), 711–717. <https://doi.org/10.1039/C5QI00263J>.
- (16) Messina, M. S.; Axtell, J. C.; Wang, Y.; Chong, P.; Wixtrom, A. I.; Kirlikovali, K. O.; Upton, B. M.; Hunter, B. M.; Shafaat, O. S.; Khan, S. I.; et al. Visible-Light-Induced Olefin Activation Using 3D Aromatic Boron-Rich Cluster Photooxidants. *J. Am. Chem. Soc.* **2016**, *138* (22), 6952–6955. <https://doi.org/10.1021/jacs.6b03568>.
- (17) Axtell, J. C.; Messina, M. S.; Liu, J.-Y.; Galaktionova, D.; Schwan, J.; Porter, T. M.; Savage, M. D.; Wixtrom, A. I.; Rheingold, A. L.; Kubiak, C. P.; et al. Photooxidative Generation of Dodecaborate-Based Weakly Coordinating Anions. *Inorg. Chem.* **2019**, *58* (16), 10516–10526. <https://doi.org/10.1021/acs.inorgchem.9b00935>.
- (18) Barton, J. L.; Wixtrom, A. I.; Kowalski, J. A.; Qian, E. A.; Jung, D.; Brushett, F. R.; Spokoyny, A. M. Perfunctionalized Dodecaborate Clusters as Stable Metal-Free Active Materials for Charge Storage. *ACS Appl. Energy Mater.* **2019**, *2* (7), 4907–4913. <https://doi.org/10.1021/acsaem.9b00610>.
- (19) Aubry, T. J.; Axtell, J. C.; Basile, V. M.; Winchell, K. J.; Lindemuth, J. R.; Porter, T. M.; Liu, J.-Y.; Alexandrova, A. N.; Kubiak, C. P.; Tolbert, S. H.; et al. Dodecaborane-Based Dopants Designed to Shield Anion Electrostatics Lead to Increased Carrier Mobility in a Doped Conjugated Polymer. *Adv. Mater.* **2019**, *31* (11), 1805647. <https://doi.org/10.1002/adma.201805647>.
- (20) Axtell, J. C.; Saleh, L. M. A.; Qian, E. A.; Wixtrom, A. I.; Spokoyny, A. M. Synthesis and Applications of Perfunctionalized Boron Clusters. *Inorg. Chem.* **2018**, *57* (5), 2333–2350. <https://doi.org/10.1021/acs.inorgchem.7b02912>.

- (21) Quiroz-Guzman, M.; Brown, S. N. Tris(4-Bromo-phenyl)Aminium Hexa-chloridoantimonate ('Magic Blue'): A Strong Oxidant with Low Inner-Sphere Reorganization. *Acta Crystallogr. C* **2010**, *66* (7), m171–m173. <https://doi.org/10.1107/S0108270110019748>.
- (22) Connelly, N. G.; Geiger, W. E. Chemical Redox Agents for Organometallic Chemistry. *Chem. Rev.* **1996**, *96* (2), 877–910. <https://doi.org/10.1021/cr940053x>.
- (23) Stoll, S.; Schweiger, A. EasySpin, a Comprehensive Software Package for Spectral Simulation and Analysis in EPR. *J. Magn. Reson.* **2006**, *178* (1), 42–55. <https://doi.org/10.1016/j.jmr.2005.08.013>.

*Intentionally left blank*